Alumina nanoparticles induce expression of endothelial cell adhesion molecules

Elizabeth Oesterling[a], Nitin Chopra[b], Vasileios Gavalas[b], Xabier Arzuaga[c], Eun Jin Lim[c], Rukhsana Sultana[b], D. Allan Butterfield[b], Leonidas Bachas[b], Bernhard Hennig[a,c,*]

[a] Graduate Center for Toxicology, University of Kentucky, Lexington, KY 40536, United States
[b] Department of Chemistry and Center of Membrane Sciences, University of Kentucky, Lexington, KY 40536, United States
[c] Molecular and Cell Nutrition Laboratory, College of Agriculture, University of Kentucky, Lexington, KY 40536-0200, United States

ARTICLE INFO

ABSTRACT

Nanotechnology is a rapidly growing industry that has elicited much concern because of the lack of available toxicity data. Exposure to ultrafine particles may be a risk for the development of vascular diseases due to dysfunction of the vascular endothelium. Increased endothelial adhesiveness is a critical first step in the development of vascular diseases, such as atherosclerosis. The hypothesis that alumina nanoparticles increase inflammatory markers of the endothelium, measured by the induction of adhesion molecules as well as the adhesion of monocytes to the endothelial monolayer, was tested. Following characterization of alumina nanoparticles by transmission electron microscopy (TEM), electron diffraction, and particle size distribution analysis, endothelial cells were exposed to alumina at various concentrations and times. Both porcine pulmonary artery endothelial cells and human umbilical vein endothelial cells showed increased mRNA and protein expression of VCAM-1, ICAM-1, and ELAM-1. Furthermore, human endothelial cells treated with alumina particles showed increased adhesion of activated monocytes. The alumina particles tended to agglomerate at physiological pH in serum-containing media, which led to a range of particle sizes from nano to micron size during treatment conditions. These data show that alumina nanoparticles can elicit a proinflammatory response and thus present a cardiovascular disease risk.

© 2008 Published by Elsevier Ireland Ltd.

1. Introduction

Nanotechnology is a fast growing industry with seemingly limitless applications from cosmetics and skin care products to abrasives and polishers to drug delivery devices. Manufactured nanoparticles (MNPs), materials created in the diameter range of <100 nm, display unique physicochemical characteristics due in part to their smaller size, large surface-to-volume ratio, and increased reactivity. These changes in characteristics could cause a generally bioinert material to behave differently at the nanoscale. Alumina, or aluminum oxide, is among the most abundantly produced nanosized particles, estimated to account for approximately 20% of the 2005 world market of nanoparticles (Rittner, 2002). Because of the extreme potential of MNP and their increased usage, occupational and public exposure will dramatically increase in the future. Future estimates of engineered nanoparticle production rates anticipate that by the year 2011, rates could increase to 58,000 metric tons produced per year

(Maynard, 2006). With this in mind, there has been a recent emergence of concern dealing with the potential for toxicity and the lack of data to substantiate or dismiss these concerns (Oberdorster et al., 2005; Thomas and Sayre, 2005; Borm et al., 2006; Maynard, 2007a,b).

It has been shown that inhaled nanosized particles can travel into the bloodstream, possibly through the "gap fenestration pathway" at the air–blood barrier where gaps from 0.03 to 3 μm between alveolar epithelial cells have been visualized (Shimada et al., 2006), thus allowing for particle interaction with luminal cell types, such as the vascular endothelium, and entering into extrapulmonary tissues (Artelt et al., 1999; Takenaka et al., 2001; Nemmar et al., 2002). Inflammation or dysfunction of the endothelial layer is considered to be an initiating event for the development of vascular diseases, such as atherosclerosis (Nabel, 1991; Glass and Witztum, 2001; Libby, 2002). Increased adhesiveness of the endothelium leads to the recruitment and extravasation of leukocytes from the lumen into the vessel intima, where the leukocytes could engulf oxidized lipid particles and develop into inflammatory foam cells. These processes can be monitored in vitro by measuring inflammatory markers such as vascular cellular adhesion molecule-1 (VCAM-1), intercellular adhesion molecule-1 (ICAM-1), and P- and E-selectins (ELAM-1). Nanoparticles may play a role in exacerbating or accelerating this critical first step toward vascular disease.

* Corresponding author at: Molecular and Cell Nutrition Laboratory, College of Agriculture, University of Kentucky, Room 591 Wethington Health Sciences Building, 900 S. Limestone, Lexington, KY 40536-0200, United States. Tel.: +1 859 323 4933x81343; fax: +1 859 257 1811.
E-mail address: bhennig@uky.edu (B. Hennig).

It has been shown that after intratracheal instillation in rats, treatment with TiO_2 particles caused increased rolling and adhesion of polymorphonuclear leukocytes to the luminal surface of systemic venules (Nurkiewicz et al., 2006). Further, alumina nanoparticles have been shown to initiate inflammatory events in macrophages, including secretion of proinflammatory cytokines and interaction with neighboring cell types (Yagil-Kelmer et al., 2004; Rodrigo et al., 2006) that could also lead to activation of the endothelium. The development of endothelial adhesiveness is mediated by a number of adhesion molecules, such as VCAM-1 (Cybulsky and Gimbrone, 1991), ICAM-1 (Collins et al., 2000), and ELAM-1 (Dong et al., 1998). A recent paper demonstrated that metal oxide nanoparticles can lead to dysfunction of the endothelium, but that this process was dependent upon the particle composition (Gojova et al., 2007). Iron oxide (Fe_2O_3), yttrium oxide (Y_2O_3), and zinc oxide (ZnO) were all internalized into human aortic endothelial cells, but only Y_2O_3 and ZnO were able to induce the expression of ICAM-1, interleukin-8, or monocyte chemotactic protein-1.

It was hypothesized that MNP, such as alumina, lead to increased endothelial cell dysfunction, evidenced by increased inflammatory processes. This was tested in both human umbilical vein endothelial cells and primary porcine pulmonary artery endothelial cells. Cells were exposed to commercially bought alumina for up to 40 h, and various measures of cellular adhesion were analyzed.

2. Materials and methods

2.1. Materials

Antibodies used were anti-VCAM-1 (clone 1.G11B1, Millipore, Billercia, MA), anti-ICAM-1 (clone RR1/1, Invitrogen, Carlsbad, CA), anti-ELAM-1 (clone 1.2B6, Chemicon International, CA), and anti-GAPDH (Santa Cruz Biotechnology, Santa Cruz, CA). Anti-rabbit, anti-mouse, and anti-goat secondary antibodies were purchased from Santa Cruz Biotechnology (Santa Cruz, CA). Alexafluor 488 and 546 conjugated secondary antibodies were purchased from Invitrogen (Molecular Probes, Carlsbad, CA).

2.2. Nanoparticle characterization

The alumina nanoparticles used in this study were obtained from Alfa Aesar (Ward Hill, MA; alumina oxide, γ–α, 99.98% purity, 10–20 nm, stock# 10459, Lot# I20G14). The polystyrene nanoparticles were obtained from Spherotech (Lake Forest, IL; PP-008, 0.05–0.1 μm). Alumina particles were weighed and autoclaved for 15 min at 121 °C. Experimental media were added, and the nanoparticle dispersion was characterized by using a particle size distribution (PSD) analyzer, transmission electron microscopy (TEM), and electron diffraction. There was no change in the structural and physical characteristics of alumina nanoparticles after autoclaving. This was confirmed by TEM and electron diffraction studies before and after this process. The latter also revealed presence of similar phases (α-, γ-, and κ-Al_2O_3) in the autoclaved and non-autoclaved nanoparticles. In addition, high resolution TEM indicated no change in the lattice of the autoclaved and non-autoclaved nanoparticles.

For the PSD, nanoparticles were dispersed in the media and vortexed. Subsequently, 5 ml of the dispersion was added to a quartz cuvette, and placed in the Brookhaven 90Plus Nanoparticle size analyzer (Brookhaven Instruments, Holtsville, NY). Fluctuations of the scattered light due to the random motion of the particles fluctuations were measured and converted into particle diameter. The scattering angle in the experiments was set at 90°, particle refractive index was 1.761, and the viscosity of the solution was assumed to be 1.2 cP. It has been previously reported that the viscosity of 10% fetal bovine serum (FBS) is close to that of ethanol, which is 1.2 cP (Hahn, 2000; Xie et al., 2006). The experiment was allowed to run for 90 min, and the software automatically generated the diameter distribution in a multimodal mode.

For the TEM, a drop of the nanoparticle suspension was placed on a 200 mesh Cu-lacy carbon TEM grid (EM Sciences, Hatfield, PA). The droplet on the grid was allowed to dry overnight in a vacuum oven at room temperature. After evaporation, the alumina nanoparticles were dispersed on the TEM grid. TEM measurements were performed in a JEOL 2010f instrument (JEOL, Tokyo, Japan) with operating voltage of 200 kV. The electron diffraction experiment was performed on the same sample used for TEM. The diffraction pattern and indexing was obtained using DigitalMicrograph imaging software (Gatan, Pleasanton, CA) interfaced with the microscope. The indexed rings and the alumina phases were further confirmed with the standard Joint Committee on Powder Diffraction International Centre for Diffraction Data (JCPDS-ICCD).

2.3. Cell culture

Both primary porcine arterial endothelial cells (PECs) and primary human umbilical vein endothelial cells (HUVECs) were used in these experiments as models to evaluate inflammatory cardiovascular disease. Cells were isolated from porcine pulmonary arteries and human umbilical cord veins, respectively, as explained previously (Toborek et al., 2002). Human umbilical cords were obtained from the University of Kentucky Labor and Delivery unit. Porcine endothelial cells were cultured in M199 (GIBCO Laboratories, Grant Island, NY), supplemented with 10% FBS (Hyclone Laboratories, Logan, UT). HUVECs were cultured in M199 supplemented with 20% FBS as described previously (Toborek et al., 2002).

2.4. Experimental conditions

Cells were supplemented with autoclaved alumina particles or polystyrene particles at a concentration of 1.0–250 μg/ml, and then events of endothelial cell dysfunction were measured. One of the hallmarks of endothelial cell dysfunction is increases in endothelial cell adhesiveness. The experimental media for PECs and HUVECs contained 1% or 10% FBS, respectively. Alumina exposure is also represented as mass per culture dish surface area to more accurately represent the experimental conditions. Conversion of treatment groups to mass per culture dish surface area corresponds to treatments of 1.4–350 ng/mm^2.

2.5. Western blotting

Whole-cell lysates were prepared with a lysis buffer containing 50 mM Tris–HCl (pH 8.0), 200 mM NaCl, 20 mM EDTA, 1% SDS, 0.5% Na–deoxycholic acid, 0.01% NP-40, 200 mM sodium orthovanadate, and 100 mM phenylmethylsulfonyl fluoride. Equal amounts of protein (40 μg) were fractionated by SDS-polyacrylamide gel electrophoresis and transferred to nitrocellulose membranes. The membrane was blocked at room temperature with 5% non-fat milk in Tris-buffered saline (TBS, pH 7.6) containing 0.05% Tween 20, and then washed with TBS-Tween. VCAM-1, ICAM-1, and GAPDH antibodies were incubated at 4 °C overnight at a 1:1000 dilution in 5% bovine serum albumin in TBS-Tween. Horseradish peroxidase-conjugated secondary antibodies were incubated for 1 h at a 1:3000 dilution. Bands were visualized by using ECL immunoblotting detection reagents (Amersham Biosciences, Buckinghamshire, England). Bands were quantified using UN-SCAN-IT gel Version 5.1 (Silk Scientific, Orem, UT) and normalized to GAPDH protein expression.

2.6. Immunofluorescence

Endothelial cells were grown to confluency on glass culture slides and incubated with or without alumina (100 μg/ml) or with TNF-α (10 ng/ml; Sigma) for 24 h. After three washes in phosphate-buffered saline (PBS), cells were treated with 50:50 acetone:methanol for 30 min. After 45 min of blocking of non-specific binding with PBS containing 1% bovine serum albumin (BSA), cells were incubated with VCAM-1, ICAM-1, or ELAM-1 primary antibodies (for 30 min at 37 °C, dilution of 1:50) and were washed twice in PBS. Then, they were incubated simultaneously with Alexafluor 546 or 488-labeled secondary antibody (15 min at 37 °C, dilution of 1:200). Three negative controls were prepared by incubation of the cells with secondary antibody species-specific IgG, no primary antibody added, or no primary and secondary antibody added. The cells were washed twice in PBS and stained with Hoechst 33342 dye (for 5–10 min at 37 °C, concentration 1 μg/ml). The stained slides were mounted in aqueous mounting medium before being visualized and captured using an Olympus BX61WI confocal microscope and FluoView software.

2.7. Real-time PCR

Porcine endothelial cells were treated with alumina (100 μg/ml) for 4 h and 8 h. Total RNA was extracted from cells using Trizol reagent (Invitrogen, Carlsbad, CA, USA) according to the manufacturer's instructions and then reverse transcribed into cDNA using the Reverse Transcription System (Promega, Madison, WI, USA). VCAM-1 and ELAM-1 gene expression changes were analyzed using quantitative real-time PCR and SYBR Green technology (ABI 7300, Applied Biosystems, Foster City, CA, USA). Real-time PCR was conducted using 100 ng cDNA, 12.5 μl 2× SYBR Green PCR Master Mix (Applied Biosystems), and 150 pmol of forward and reverse primers (Integrated DNA Technologies, Coralville, IA, USA) in a total volume of 25 μl. The sequences of primer pairs used were as follows: porcine VCAM-1 (sense, 5′-ACACCACCCCAGTCACCATATC-3′; antisense, 5′-TGGAAAGACATGGCTGCCTAT-3′), porcine ELAM-1 (sense, 5′-TGATCTTCCTGATTCCAATCCA-3′; antisense, 5′- ACACATCTGGTCGCAATTCAAA-3′), and porcine β-actin, used as an internal control (sense, 5′-TCATCACCATCGGCAACT-3′; antisense, 5′-TTCCTGATGTCCACGTCGC-3′). The following thermocycling conditions were used: 50 °C for 2 min, 95 °C for 10 min, followed by 95 °C for 15 s and 60 °C for 60 s for 40 cycles. The standard curve was generated by plotting the threshold cycle (Ct) versus the log concentration of the serial dilutions of one specific cDNA sample, which served as a calibrator. All samples were prepared in duplicate; their concentrations were calculated based on the standard curve and normalized to β-actin mRNA expression.
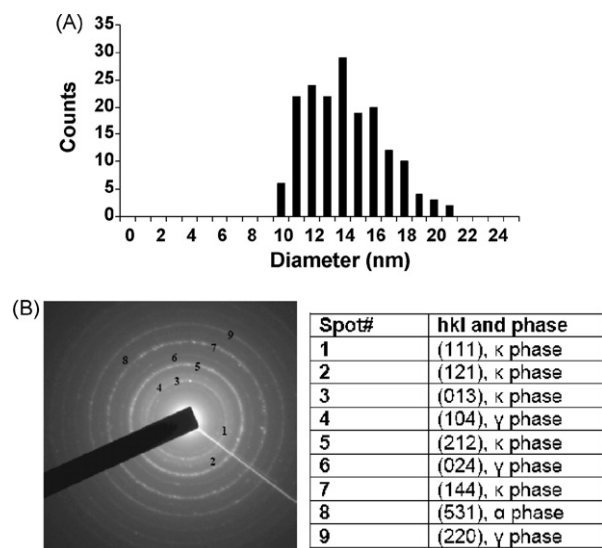
Fig. 1. Diameter distribution and electron diffraction pattern of alumina nanoparticles. Diameter distribution of TEM images indicated the size of alumina nanoparticles to be between 10 nm and 20 nm. (A) Electron diffraction data indicated the presence of three different phases of alumina nanoparticles. Results were verified and confirmed using standard data obtained from the International Centre for Diffraction Data (ICDD) database (B).

2.8. Monocyte adhesion

Human THP-1 monocytes (50,000 cells) were activated with TNF-α (10 min) and loaded with the fluorescent probe calcein (Molecular Probes, Carlsbad, CA). HUVECs were treated with 14 ng/mm^2 or 140 ng/mm^2 alumina particles for 8 h. Monocytes were added to treated endothelial cell monolayers and incubated (30 min), allowing for monocyte adhesion. Unbound monocytes were washed away, and the monolayer was fixed with 1% glutaraldehyde. Attached fluorescent monocytes were counted using a fluorescent microscope (Olympus IX70, Center Valley, PA).

2.9. Statistical analysis

Values are reported as means ± standard error of the mean (S.E.M.) of at least three independent groups. Comparisons between treatments were made by one-way analysis of variance followed by Holm-Sidak multiple comparison tests using SigmaStat 3.0 software (Systat Software, San Jose, CA). Statistical probability of $p < 0.05$ was considered significant.

3. Results

3.1. Alumina nanoparticle characterization and stability

The alumina particles were characterized by TEM and electron diffraction. The diameter of particles was observed in TEM images and the size distribution was found to be comparable to the size reported by the manufacturer of 10–20 nm (Fig. 1A). The TEM images show alumina nanoparticles in both agglomerated and non-agglomerated states (data not shown). Dynamic light scattering experiments confirmed the presence of particle agglomerates greater than 500 nm in diameter in the presence of FBS media; nevertheless, a significant portion of alumina was still present as non-agglomerated nanoparticles of less than 100 nm in size. Electron diffraction indicated the presence of α-, γ-, and κ-Al$_2$O$_3$ (Fig. 1B). Alumina can exist in many forms, α, χ, η, δ, κ, θ, γ, ρ; these arise during the heat treatment of aluminum hydroxide or aluminum oxy hydroxide during the synthesis of alumina nanoparticles. The most thermodynamically stable form is α-Al$_2$O$_3$.

3.2. Alumina increases endothelial adhesion molecule expression

Alumina particles induced protein expression of VCAM-1 (Fig. 2A) and ICAM-1 (Fig. 2B) in a time-dependent manner in both

HUVECs and porcine endothelial cells (data not shown) treated with 140 ng/mm^2 alumina. This adhesion molecule induction was also dose-dependent with significant increases in VCAM-1 after treatment with 140 ng/mm^2 alumina (Fig. 3A) and ICAM-1 after treatment with 70 ng/mm^2 or 140 ng/mm^2 alumina (Fig. 3B). The same up-regulation was not seen in cells treated with polystyrene particles at the same and higher concentrations (Fig. 3). The similar concentration dependent trend was seen in additional inflammatory endpoints examined including cyclooxygenase-2 (data not shown). Cytotoxicity experiments showed that concentrations of alumina particles above 1400 ng/mm^2 led to overt cell death shown by MTT assay and changes in cell morphology. For this reason further experiments were conducted at 140 ng/mm^2, where no detectable cell death occurred.

Alumina particles also induced mRNA expression of both VCAM-1 (Fig. 4A) and ELAM-1 (Fig. 4B) in porcine endothelial cells after 4 h and 8 h of treatment at a culture dish surface area dose of 140 ng/mm^2 (1.4 g/cm^2). VCAM-1 had a higher induction after 4 h of treatment than after 8 h once normalized to β-actin. ELAM-1 had a higher induction after 8 h, than after 4 h.

The increased adhesion molecule protein expression resulting from alumina treatment was also visualized by immunofluorescence staining (Fig. 5). Alumina increased VCAM-1, ICAM-1, and ELAM-1 after 24 h of treatment (100 μg/ml or 250 ng/mm^2) shown in porcine endothelial cells and HUVECs, respectively, as did TNF-α, which was used as a positive control. Increased VCAM-1, ICAM-1, and ELAM-1 protein staining was visualized in both cell types.
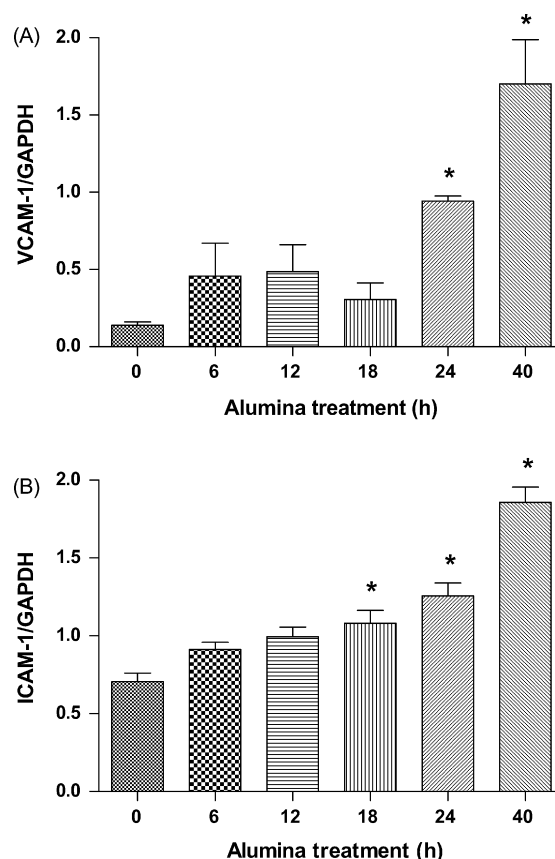

Fig. 2. Alumina increases VCAM-1 and ICAM-1 protein expression in a time-dependent manner. HUVECs were treated with 140 ng/mm^2 (100 μg/ml) alumina particles for 0–40 h. Whole-cell lysates were analyzed by immunoblot for VCAM-1 (A), ICAM-1 (B), and GAPDH. Bars represent average and S.E.M. of at least three independent groups normalized to GAPDH. *$p < 0.05$ compared to control cultures.
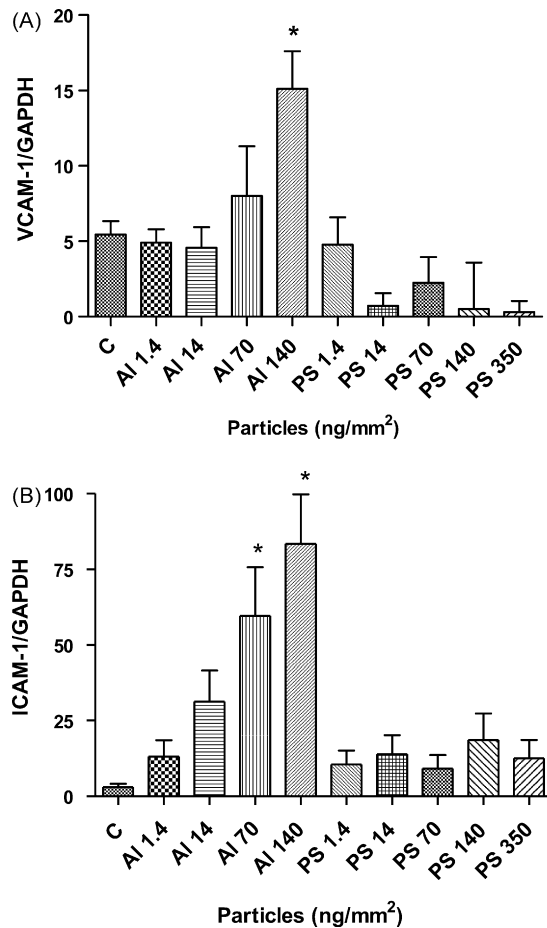
Fig. 3. Alumina increases VCAM-1 and ICAM-1 protein expression in a dose-dependent manner. HUVECs were treated with alumina (Al) or polystyrene (PS) particles for 24 h, at varying concentrations (1.4–350 ng/mm², 1–250 μg/ml). Whole-cell lysates were analyzed by immunoblot for VCAM-1 (A), ICAM-1 (B), and GAPDH. Bars represent average and S.E.M. of at least three independent groups normalized to GAPDH. *$p < 0.05$ compared to control cultures.

3.3. Alumina increases monocyte adhesion to endothelium

Alumina treatment was also found to increase the adhesion of activated monocytes onto the endothelial cell monolayer (Fig. 6). Fixed, adherent fluorescently labeled THP-1 monocytes were counted. There was a statistically significant increase in adhered monocytes when the endothelium was treated with either 14 ng/mm² or 140 ng/mm² alumina.

4. Discussion

There is an evidence suggesting that exposure to ultrafine particulate air pollution (<100 nm) is linked to increased incidence of cardiovascular diseases (Wichmann et al., 2000; Ibald-Mulli et al., 2002; Peters and Pope, 2002; Lanki et al., 2006). It is thus conceivable that human exposure to manufactured particulate matter in this size range also presents a risk to consumers as well as to occupational workers. The mechanisms leading to the increased cardiovascular risks have not been fully elucidated, but endothelial cell dysfunction and inflammation is a key step toward the progression of vascular diseases and has been shown to be associated with air pollution effects (van Eeden et al., 2005; Hansen et al., 2007; O'Neill et al., 2007). With this in mind, it was hypothesized that MNP, such as alumina, lead to increased endothelial cell dysfunction, evidenced by increased endothelial adhesiveness. Endothelial

adhesion molecules are responsible for migration of leukocytes into the vessel, where the leukocytes develop into inflammatory foam cells evident in atherosclerotic fatty streaks. Results in the current study demonstrated that direct exposure of endothelial cells to alumina nanoparticles increased adhesion molecule mRNA and protein expression in a dose- and time-dependent manner as well as increased adhesion of activated monocytes to the endothelial cell monolayer. The mechanisms behind these events are not well understood.

One possibility for the induction of adhesion molecules is the production of reactive oxygen species (ROS) and the activation of redox sensitive signaling pathways. Preliminary experiments on the effects of alumina on both 4-hydroxynonenal (4-HNE) and protein carbonyl production did not reveal significant increases in ROS production (data not shown). These results are in agreement with recent studies suggesting that certain other metal oxide nanoparticles have not significantly promoted ROS upon internalization into cells (Schubert et al., 2006; Xia et al., 2006; Gojova et al., 2007). Nuclear factor-kappa B (NF-κB) is part of one known pathway that leads to the production of inflammatory adhesion molecules like VCAM-1, ICAM-1, and ELAM-1 (Iademarco et al., 1992; Schindler and Baichwal, 1994). Preliminary studies on the role of NF-κB were also conducted using the irreversible NF-κB inhibitor (E)3-[(4-*t*-butylphenyl)sulfonyl]-2-propenenitrile (BAY 11-7085), which acts by preventing the phosphorylation, and thus release and degradation of IκBα, the endogenous inhibitory NF-κB regulatory protein (Pierce et al., 1997). The results suggest that NF-κB inhibition did not change the magnitude of induction of VCAM-1
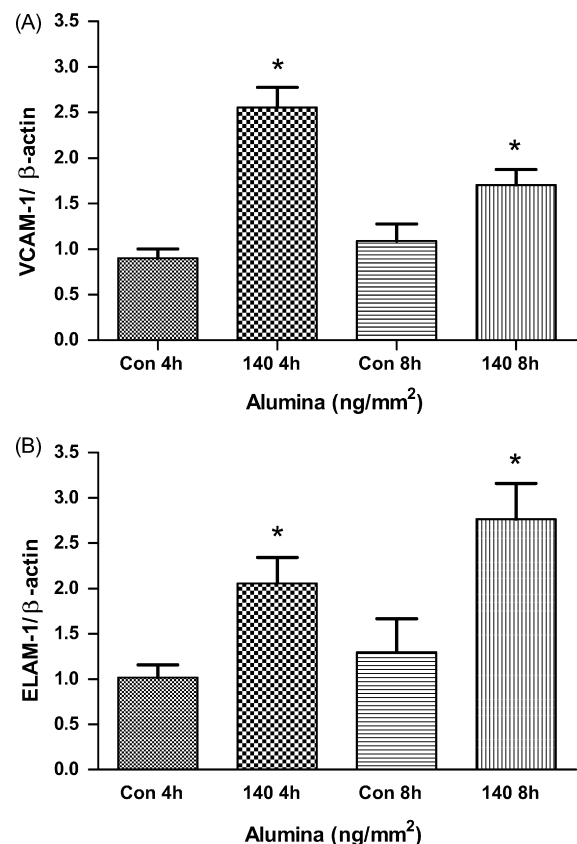

Fig. 4. Alumina increases ELAM-1 and VCAM-1 mRNA expression. Porcine endothelial cells (PECs) were treated with 140 ng/mm² alumina particles for 4 h and 8 h. VCAM-1 (A) and ELAM-1 (B) expression was analyzed using quantitative real-time PCR and SYBR Green technology. Bars represent average and S.E.M. of at least three independent groups normalized to β-actin. *$p < 0.05$ compared to corresponding time control cultures.
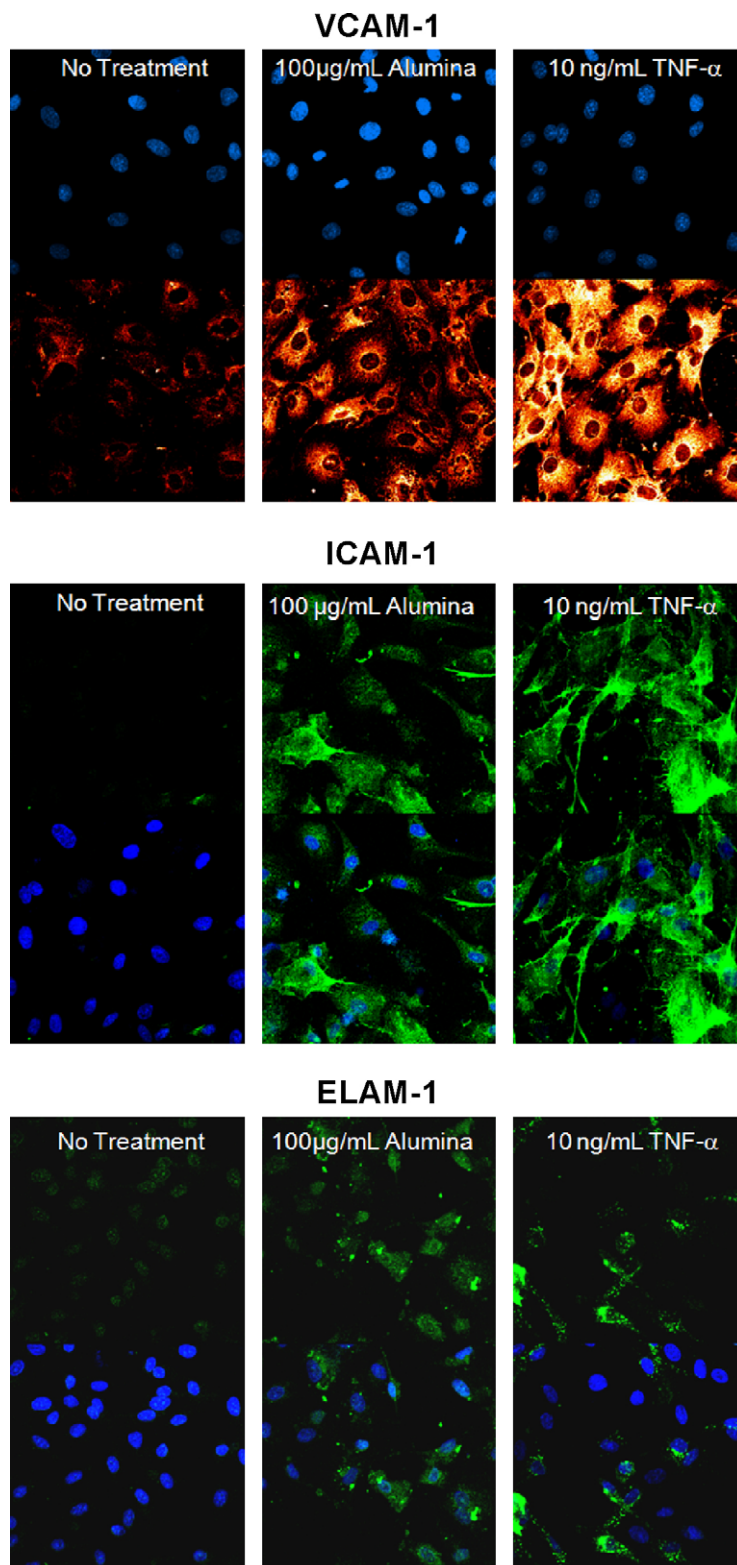
VCAM-1

ICAM-1

ELAM-1

Fig. 5. Alumina increases adhesion molecule protein expression. PECs and HUVECs were treated with 100 μg/ml alumina particles or 10 ng/ml TNF-α for 24 h. Cells were fixed and probed for VCAM-1 (PEC), ICAM-1 (HUVEC), or ELAM-1 (HUVEC) using AlexaFluor antibodies. VCAM-1 staining is shown as orange, ICAM-1 and ELAM-1 as green, and nuclei are stained with Hoechst 33342 in blue. Samples were visualized and captured using an Olympus BX61WI confocal microscope. Images are representative of multiple treatment groups between both cell types. (For interpretation of the references to color in this figure legend, the reader is referred to the web version of the article.)

over control; thus, VCAM-1 induction is possibly not through the NF-κB pathway. Other signaling pathway options have not been investigated, however, a number of possibilities exist including specificity protein-1 (SP-1) (Neish et al., 1995a,b; Zhang and Frei, 2003), activator protein-1 (AP-1) (Verna et al., 2006), and interferon regulatory factor (IRF-1) (Neish et al., 1995a,b; Dagia et al., 2004), which can operate solely or in unison to promote adhesion molecule up-regulation.
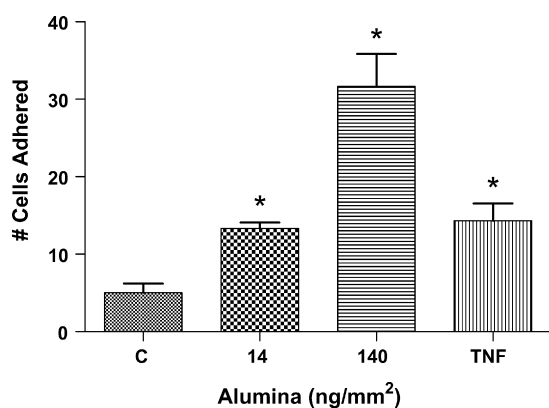
Fig. 6. Alumina increases monocyte adhesion to endothelial monolayers. Human THP-1 monocytes were activated with TNF-α (10 min) and loaded with the fluorescent probe calcein. HUVECs were treated with 140 ng/mm^2 or 14 ng/mm^2 alumina particles for 8 h. Monocytes were added to treated endothelial cell monolayers, allowing for monocyte adhesion. Attached fluorescent monocytes were counted using a fluorescent microscope (Olympus IX70). $^*p < 0.05$ compared to control cultures.

Recent studies have also shown that MNPs may play a proinflammatory role once exposed to endothelial cells. Carbon black particles were shown to induce monocyte chemoattractant protein-1 (MCP-1) in human endothelial cells and reduce the expression of endothelial nitric oxide synthase, important for the contractive properties of the endothelium (Yamawaki and Iwai, 2006). A recent study also showed the induction of MCP-1 along with ICAM-1 and IL-8 in endothelial cells treated with ZnO or Y_2O_3 nanoparticles (Gojova et al., 2007).

The alumina particles used were measured to be around 10–20 nm as provided by the manufacturer data and confirmed by TEM. When added to culture media that includes serum proteins, larger agglomerates were found in addition to smaller nanoparticles as has been shown by other groups before (Wagner et al., 2007). These particles and smaller aggregates were in the size range of particles that could enter the cell through endocytosis (Liu and Shapiro, 2003). It is likely that exposure to these larger agglomerated nanoparticle units is a physiologically relevant scenario. Indeed, many toxicity studies on nanoparticles in animals were carried out with aggregated or agglomerated particles instead of individual nanoparticles, yet still observed nanoparticle based effects (Maynard, 2007a,b). Mathematical models have predicted that 10%–20% of respired particles between 0.1 μm and 1 μm in diameter reach the alveolar regions of the lungs where they can come in contact with the circulation (Oberdorster et al., 2005). These models were based on singlet particle exposure; still alumina aggregates in the current study were found in this size range, suggesting again that both the aggregated and non-aggregated particles may lead to toxic events and enter the circulation.

Experiments in the current study were conducted in two primary endothelial cell types. Similar results were observed in both cultures; however, human cells seemed more sensitive to nanoparticle exposure compared to porcine derived cells. As these experiments were conducted in vitro, other elements characteristic of physiological exposure could not be modeled. For example, endothelial cells in vivo are constantly exposed to flow conditions, which will likely change the delivery and interactions between nanoparticles and the vascular wall (Blackwell et al., 2001). Endothelial cells also work in concert with various other cell types including leukocytes and smooth muscle cells. The effects of nanosized alumina on these cell types could also cause inflammatory changes in the endothelium. Another area of interest is the concentration that actually enters the circulation and comes in con-

tact with the endothelium. The amount of translocation of particles from the lung into the circulation has not been fully explained. It has been shown that nanoparticles do enter the circulation and extrapulmonary tissues (Nemmar et al., 2001, 2002; Oberdörster et al., 2002) with possibly up to 15% of the inhaled dose reaching the capillaries (Geiser et al., 2005).

In summary, data from the current study demonstrate that alumina nanoparticles cause increased adhesiveness shown by induction of VCAM-1, ICAM-1, and ELAM-1 as well as increased monocyte adhesion to vascular endothelial cells. These data suggest that exposure to nanoparticles may be a significant risk for the development of inflammatory diseases such as atherosclerosis.

Conflict of interest

The authors have no conflict of interest.

Acknowledgments

References

Artelt, S., Creutzenberg, O., Kock, H., Levsen, K., Nachtigall, D., Heinrich, U., Rühle, T., Schlögl, R., 1999. Bioavailability of fine dispersed platinum as emitted from automotive catalytic converters: a model study. Sci. Total Environ. 228, 219–242.

Blackwell, J.E., Dagia, N.M., Dickerson, J.B., Berg, E.L., Goetz, D.J., 2001. Ligand coated nanosphere adhesion to E- and P-selectin under static and flow conditions. Ann. Biomed. Eng. 29, 523–533.

Borm, P.J., Robbins, D., Haubold, S., Kuhlbusch, T., Fissan, H., Donaldson, K., Schins, R., Stone, V., Kreyling, W., Lademann, J., Krutmann, J., Warheit, D., Oberdorster, E., 2006. The potential risks of nanomaterials: a review carried out for ECETOC. Part. Fibre Toxicol. 3, 1–35.

Collins, R.G., Velji, R., Guevara, N.V., Hicks, M.J., Chan, L., Beaudet, A.L., 2000. P-Selectin or intercellular adhesion molecule (ICAM)-1 deficiency substantially protects against atherosclerosis in apolipoprotein E-deficient mice. J. Exp. Med. 191, 189–194.

Cybulsky, M.I., Gimbrone Jr., M.A., 1991. Endothelial expression of a mononuclear leukocyte adhesion molecule during atherogenesis. Science 251, 788–791.

Dagia, N.M., Harii, N., Meli, A.E., Sun, X., Lewis, C.J., Kohn, L.D., Goetz, D.J., 2004. Phenyl methimazole inhibits TNF-alpha-induced VCAM-1 expression in an IFN regulatory factor-1-dependent manner and reduces monocytic cell adhesion to endothelial cells. J. Immunol. 173, 2041–2049.

Dong, Z.M., Chapman, S.M., Brown, A.A., Frenette, P.S., Hynes, R.O., Wagner, D.D., 1998. The combined role of P- and E-selectins in atherosclerosis. J. Clin. Invest. 102, 145–152.

Geiser, M., Rothen-Rutishauser, B., Kapp, N., Schürch, D., Kreyling, W., Schulz, H., Semmler, M., Hof, V.I., Heyder, J., Gehr, P., 2005. Ultrafine particles cross cellular membranes by nonphagocytic mechanisms in lungs and in cultured cells. Environ. Health Perspect. 113, 1555–1560.

Glass, C.K., Witztum, J.L., 2001. Atherosclerosis: the road ahead. Cell 104, 503–516.

Gojova, A., Guo, B., Kota, R.S., Rutledge, J.C., Kennedy, I.M., Barakat, A.I., 2007. Induction of inflammation in vascular endothelial cells by metal oxide nanoparticles: effect of particle composition. Environ. Health Perspect. 115, 403–409.

Hahn, A.F., 2000. Intravenous immunoglobulin treatment in peripheral nerve disorders—indications, mechanisms of action and side-effects. Curr. Opin. Neurol. 13, 575–582.

Hansen, C.S., Sheykhzade, M., Møller, P., Folkmann, J.K., Amtorp, O., Jonassen, T., Loft, S., 2007. Diesel exhaust particles induce endothelial dysfunction in apoE−/− mice. Toxicol. Appl. Pharmacol. 219, 24–32.

Iademarco, M.F., McQuillan, J.J., Rosen, G.D., Dean, D.C., 1992. Characterization of the promoter for vascular cell adhesion molecule-1 (VCAM-1). J. Biol. Chem. 267, 16323–16329.

Ibald-Mulli, A., Wichmann, H.E., Kreyling, W., Peters, A., 2002. Epidemiological evidence on health effects of ultrafine particles. J. Aerosol. Med. 15, 189–201.

Lanki, T., Pekkanen, J., Aalto, P., Elosua, R., Berglind, N., D'Ippoliti, D., Kulmala, M., Nyberg, F., Peters, A., Picciotto, S., Salomaa, V., Sunyer, J., Tiittanen, P., Klot, S.V., Forastiere, F., 2006. Associations of traffic related air pollutants with hospitalisation for first acute myocardial infarction: the HEAPSS study. Occup. Environ. Med. 63, 844–851.

Libby, P., 2002. Inflammation in atherosclerosis. Nature 420, 868–874.

Liu, J., Shapiro, J.I., 2003. Endocytosis and signal transduction: basic science update. Biol. Res. Nurs. 5, 117–128.

Maynard, A.D., 2006. Nanotechnology: A Research Strategy for Addressing Risk. Woodrow Wilson International Center for Scholars, Washington, DC.

Maynard, A.D., 2007a. Nanotechnology: the next big thing, or much ado about nothing? Ann. Occup. Hyg. 51, 1–12.

Maynard, A.D., 2007. Is Engineered Nanomaterial Exposure a Myth? October Featured Article. www.safenano.org.

Nabel, E.G., 1991. Biology of the impaired endothelium. Am. J. Cardiol. 68, 6C–8C.

Neish, A.S., Khachigian, L.M., Park, A., Baichwal, V.R., Collins, T., 1995a. Sp1 is a component of the cytokine-inducible enhancer in the promoter of vascular cell adhesion molecule-1. J. Biol. Chem. 270, 28903–28909.

Neish, A.S., Read, M.A., Thanos, D., Pine, R., Maniatis, T., Collins, T., 1995b. Endothelial interferon regulatory factor 1 cooperates with NF-kappa B as a transcriptional activator of vascular cell adhesion molecule 1. Mol. Cell. Biol. 15, 2558–2569.

Nemmar, A., Hoet, P.H.M., Vanquickenborne, B., Dinsdale, D., Thomeer, M., Hoylaerts, M.F., Vanbilloen, H., Mortelmans, L., Nemery, B., 2002. Passage of inhaled particles into the blood circulation in humans. Circulation 105, 411–414.

Nemmar, A., Vanbilloen, H., Hoylaerts, M.F., Hoet, P.H., Verbruggen, A., Nemery, B., 2001. Passage of intratracheally instilled ultrafine particles from the lung into the systemic circulation in hamster. Am. J. Respir. Crit. Care Med. 164, 1665–1668.

Nurkiewicz, T.R., Porter, D.W., Barger, M., Millecchia, L., Rao, K.M.K., Marvar, P.J., Hubbs, A.F., Castranova, V., Boegehold, M.A., 2006. Systemic microvascular dysfunction and inflammation after pulmonary particulate matter exposure. Environ. Health Perspect. 114, 412–419.

O'Neill, M.S., Veves, A., Sarnat, J.A., Zanobetti, A., Gold, D.R., Economides, P.A., Horton, E.S., Schwartz, J., 2007. Air pollution and inflammation in type 2 diabetes: a mechanism for susceptibility. Occup. Environ. Med. 64, 373–379.

Oberdorster, G., Oberdorster, E., Oberdorster, J., 2005. Nanotoxicology: an emerging discipline evolving from studies of ultrafine particles. Environ. Health Perspect. 113, 823–839.

Oberdörster, G., Sharp, Z., Atudorei, V., Elder, A., Gelein, R., Lunts, A., Kreyling, W., Cox, C., 2002. Extrapulmonary translocation of ultrafine carbon particles following whole-body inhalation exposure of rats. J. Toxicol. Environ. Health A 65, 1531–1543.

Peters, A., Pope III, C.A., 2002. Cardiopulmonary mortality and air pollution. Lancet 360, 1184–1185.

Pierce, J.W., Schoenleber, R., Jesmok, G., Best, J., Moore, S.A., Collins, T., Gerritsen, M.E., 1997. Novel inhibitors of cytokine-induced IkappaBalpha phosphorylation and endothelial cell adhesion molecule expression show anti-inflammatory effects in vivo. J. Biol. Chem. 272, 21096–21103.

Rittner, M.N., 2002. Market analysis of nanostructured materials. Am. Ceram. Soc. Bull. 81, 33–36.

Rodrigo, A., Vallés, G., Saldaña, L., Rodríguez, M., Martínez, M.E., Munuera, L., Vilaboa, N., 2006. Alumina particles influence the interactions of cocultured osteoblasts and macrophages. J. Orthop. Res. 24, 46–54.

Schindler, U., Baichwal, V.R., 1994. Three NF-kappa B binding sites in the human E-selectin gene required for maximal tumor necrosis factor alpha-induced expression. Mol. Cell. Biol. 14, 5820–5831.

Schubert, D., Dargusch, R., Raitano, J., Chan, S.W., 2006. Cerium and yttrium oxide nanoparticles are neuroprotective. Biochem. Biophys. Res. Commun. 342, 86–91.

Shimada, A., Kawamura, N., Okajima, M., Kaewamatawong, T., Inoue, H., Morita, T., 2006. Translocation pathway of the intratracheally instilled ultrafine particles from the lung into the blood circulation in the mouse. Toxicol. Pathol. 34, 949–957.

Takenaka, S., Karg, E., Roth, C., Schulz, H., Ziesenis, A., Heinzmann, U., Schrammel, P., Heyder, J., 2001. Pulmonary and systemic distribution of inhaled ultrafine silver particles in rats. Environ. Health Perspect. 109, 547–551.

Thomas, K., Sayre, P., 2005. Research strategies for safety evaluation of nanomaterials. Part I. Evaluating the human health implications of exposure to nanoscale materials. Toxicol. Sci. 87, 316–321.

Toborek, M., Lee, Y.W., Kaiser, S., Hennig, B., 2002. Measurement of inflammatory properties of fatty acids in human endothelial cells. Methods Enzymol. 352, 198–219.

van Eeden, S.F., Yeung, A., Quinlam, K., Hogg, J.C., 2005. Systemic response to ambient particulate matter: relevance to chronic obstructive pulmonary disease. Proc. Am. Thorac. Soc. 2, 61–67.

Verna, L., Ganda, C., Stemerman, M.B., 2006. In vivo low-density lipoprotein exposure induces intercellular adhesion molecule-1 and vascular cell adhesion molecule-1 correlated with activator protein-1 expression. Arterioscler. Thromb. Vasc. Biol. 26, 1344–1349.

Wagner, A.J., Bleckmann, C.A., Murdock, R.C., Schrand, A.M., Schlager, J.J., Hussain, S.M., 2007. Cellular interaction of different forms of aluminum nanoparticles in rat aveolar macrophages. J. Phys. Chem. B 111, 7353–7359.

Wichmann, H.E., Spix, C., Tuch, T., Wölke, G., Peters, A., Heinrich, J., Kreyling, W.G., Heyder, J., 2000. Daily mortality and fine and ultrafine particles in Erfurt, Germany. Part I. Role of particle number and particle mass. Res. Rep. Health Eff. Inst. 98, 5–86.

Xia, T., Kovochich, M., Brant, J., Hotze, M., Sempf, J., Oberley, T., Sioutas, C., Yeh, J.I., Wiesner, M.R., Nel, A.E., 2006. Comparison of the abilities of ambient and manufactured nanoparticles to induce cellular toxicity according to an oxidative stress paradigm. Nano Lett. 6, 1794–1807.

Xie, L., Jiang, Y., Yao, W., Gu, L., Sun, D., Ka, W., Wen, Z., Chien, S., 2006. Studies on the biomechanical properties of maturing reticulocytes. J. Biomech. 39, 530–535.

Yagil-Kelmer, E., Kazmier, P., Rahaman, M.N., Bal, B.S., Tessman, R.K., Estes, D.M., 2004. Comparison of the response of primary human blood monocytes and the U937 human monocytic cell line to two different sizes of alumina ceramic particles. J. Orthop. Res. 22, 832–838.

Yamawaki, H., Iwai, N., 2006. Mechanisms underlying nano-sized air-pollution-mediated progression of atherosclerosis: carbon black causes cytotoxic injury/inflammation and inhibits cell growth in vascular endothelial cells. Circ. J. 70, 129–140.

Zhang, W.J., Frei, B., 2003. Intracellular metal ion chelators inhibit TNFalpha-induced SP-1 activation and adhesion molecule expression in human aortic endothelial cells. Free Radical Biol. Med. 34, 674–682.